REPORT

OPTICS

Soliton microcomb range measurement

Myoung-Gyun Suh and Kerry J. Vahala*

Laser-based range measurement systems are important in many application areas, including autonomous vehicles, robotics, manufacturing, formation flying of satellites, and basic science. Coherent laser ranging systems using dual-frequency combs provide an unprecedented combination of long range, high precision, and fast update rate. We report dual-comb distance measurement using chip-based soliton microcombs. A single pump laser was used to generate dual-frequency combs within a single microresonator as counterpropagating solitons. We demonstrated time-of-flight measurement with 200-nanometer precision at an averaging time of 500 milliseconds within a range ambiguity of 16 millimeters. Measurements at distances up to 25 meters with much lower precision were also performed. Our chip-based source is an important step toward miniature dual-comb laser ranging systems that are suitable for photonic integration.

The invention of the optical frequency comb has had a major impact on light detection and ranging (LIDAR) systems. In addition to providing a highly accurate frequency calibration source in methods such as multiwavelength interferometry (*1*) and frequency-modulated continuous-wave laser interferometry (*2*), frequency combs have enabled a new method called dual-comb LIDAR (*3*). In this method, two frequency combs having slightly different repetition rates are phase-locked. Their combined output pulse streams then provide a LIDAR source with subnanometer precision and range ambiguity many orders beyond the pulse-to-pulse separation distance of each comb. Besides mode-locked lasers, electro-optic modulation combs have also been used in the related field of tomography (*4*). The development of miniature frequency combs [microcombs (*5*–*14*)] suggests that chip-integrated dual-comb LIDAR systems may be possible. A recent advancement in microcombs is the realization of soliton mode locking (*15*–*19*), which provides phase-locked femtosecond pulses with gigahertz to terahertz repetition rates. Soliton microcombs are being studied in several frequency comb applications, including optical frequency synthesis (*20*), optical communications (*21*), and dual-comb spectroscopy (*22*–*24*). We demonstrate time-of-flight distance measurement using a chip-based dual-soliton source. Beyond the demonstration of microcomb LIDAR, the two soliton streams are cogenerated as counterpropagating solitons within a single resonator (*25*). This simplifies the system by eliminating the need for two resonators and two pump lasers while also improving mutual coherence between the two combs. Although a close examination of systematics and other issues is not presented, the work establishes the feasibility of soliton microcombs as well as the cogeneration method for LIDAR applications.

By pumping a resonance of a silica wedge resonator (*26*) along the clockwise (CW) and counterclockwise (CCW) directions, we generated counterpropagating solitons with average power of ~1 mW (Fig. 1A). The two pumps were derived from a single 1550-nm fiber laser; after a 50/50 fiber splitter, their frequencies were controlled using acousto-optic modulators (AOMs). A feedback loop with 20-kHz bandwidth (*27*) fixes the frequency detuning of one pump relative to the cavity resonant frequency, while the second pump frequency can be independently tuned using an AOM. Chiral symmetry breaking (*28*, *29*) was observed but did not prevent counterpropagating soliton generation (*30*). Typical optical spectra of the CW and CCW solitons (Fig. 1, B and C) show the characteristic hyperbolic-secant-square spectral envelope (the green dashed curve in Fig. 1B is a fit using a soliton pulse width of 200 fs).

Fast photodetection (bandwidth 50 GHz) of the dual pulse streams as measured on an electrical spectrum analyzer (ESA) shows that the repetition frequency (f_{rep}) is approximately 9.36 GHz (Fig. 1D). A zoom-in of the electrical spectrum near f_{rep} (Fig. 1D, inset) resolves the two distinct repetition frequencies of the CW/CCW solitons. Note that the intersoliton beat notes are >40 dB lower than the repetition frequency signals and are below the electrical noise level. The repetition frequency difference (Δf_{rep}) between CW and CCW solitons is adjusted by using the AOMs to tune the frequency difference of the two pump lasers (Δf_{pump}). This repetition rate control results from the Raman-induced soliton self-frequency shift (*25*), such that Δf_{rep} increases with increasing Δf_{pump} (Fig. 1E). The maximum Δf_{rep} ~ 20 kHz is limited by the maximum Δf_{pump} ~ 3 MHz, which is set by the 3-dB frequency shift range of the AOM. Within the tunable range of Δf_{rep}, we also observed phase locking of the CW and CCW solitons and their relative repetition rates by injection locking through the backscattered light (*25*). However, the relative stability of unlocked solitons was sufficient for the time-of-flight distance measurement.

The generated CW/CCW soliton streams were coupled in opposing directions toward the LIDAR setup, with the CW soliton stream output through a gradient-index collimator toward the target mirror (Fig. 1A). A fiber delay line (physical path length ~15 m) was added before the collimator to increase the effective target distance. The CW soliton stream reflected from the target was combined with the reference CW soliton stream via a circulator and 50/50 coupler. Finally, the CW soliton stream carrying the distance information (green and orange dashed arrows) was combined with the CCW soliton stream (blue dashed arrow) to generate the periodic interference (interferogram) of the dual-soliton pulse streams. Figure 2A shows a portion of the measured interferogram as displayed by the oscilloscope. The period of the interferogram is set by the difference of the CW and CCW soliton repetition rates. The interferogram is recorded for a total of 2 s with a sampling time of 250 ns; however, only a 5-ms portion of the overall span is shown. A zoomed-in view of the interferogram (Fig. 2B) shows the reference peaks and target peaks within two periods of 176 μs, corresponding to Δf_{rep} ~ 5.685 kHz. The temporal location of the peaks in the electrical pulse stream is determined by Hilbert-transforming the interferogram. The time interval between a reference peak and a target peak is then calculated for each period and converted to the distance scale. The drift of Δf_{rep} is adaptively corrected in the data (*30*, *31*). Figure 2C plots this distance versus time where the time increment in the plot is the interferogram period (176 μs). The averaged target distance is 4.637429 mm and the range ambiguity is 16 mm (one-half of the pulse-to-pulse distance separation at a soliton repetition rate of 9.36 GHz). The right panel of Fig. 2C shows a single time period of the Hilbert-transformed interferogram near 1 s in the measurement (vertical dashed line in left panel). The inset of the right panel gives the zoomed-in target intensity peak and shows a full-width, half-maximum pulse width of ~1.45 μs. The Allan deviation of the distance time series is calculated at averaging times ranging from 352 μs to 667 ms (Fig. 3). Fitting to the plot gives $\sigma \sim 10\ \mu m\ (T_{update}/T)^{1/2}$, where T_{update} ~ 176 μs is the update time and T is the averaging time. Near an averaging time of 500 ms, a precision of 200 nm is achieved (*30*).

The distance measurement shown in Fig. 2C has a range ambiguity of 16 mm. To greatly extend this range ambiguity, we performed a similar distance measurement after manually swapping the roles of two soliton streams. In principle, this could be implemented using an integrated optical switch. The Vernier effect resulting from the difference in the soliton repetition rates can then

T. J. Watson Laboratory of Applied Physics, California Institute of Technology, Pasadena, CA 91125, USA.
*Corresponding author. Email: vahala@caltech.edu

be used to resolve the range ambiguity (*3*). Figure 4 shows a zoom-in view of the two distance measurements where R_{CW} (red) and R_{CCW} (blue) are the measured distances when the CW soliton and the CCW soliton are used for ranging. The average distance difference, ΔR = mean(R_{CW}) − mean(R_{CCW}), between the two measurements is 16.02 μm. Considering the Vernier effect (*3*), the ambiguity-resolved distance is $R' = \Delta R(f_{rep}^{CCW}/\Delta f_{rep}) + R_{CW} \approx$ 26.3729 ± 0.466 m, with a new range ambiguity of ~26 km. This measured distance is in good agreement with the optical path length of the target (~26.815 m), including fiber delay, as measured using an optical time-domain reflectometer. The uncertainty (±0.466 m) in this partially ambiguity-resolved measurement results from the original 200-nm precision multiplied by $\sqrt{2}f_{rep}/\Delta f_{rep}$. If this uncertainty were below the pulse-to-pulse range ambiguity, which would require a precision of $(c\Delta f_{rep})/(2\sqrt{2}f_{rep}^2)$ (6.88 nm in this experiment), then a nanometer-scale precision would be possible in the fully ambiguity-resolved case (*3*). In addition to the time-of-flight measurement, complementary interferometric measurement using phase-locked CW/CCW solitons could improve the precision. Finally, increasing Δf_{rep} would improve the precision by

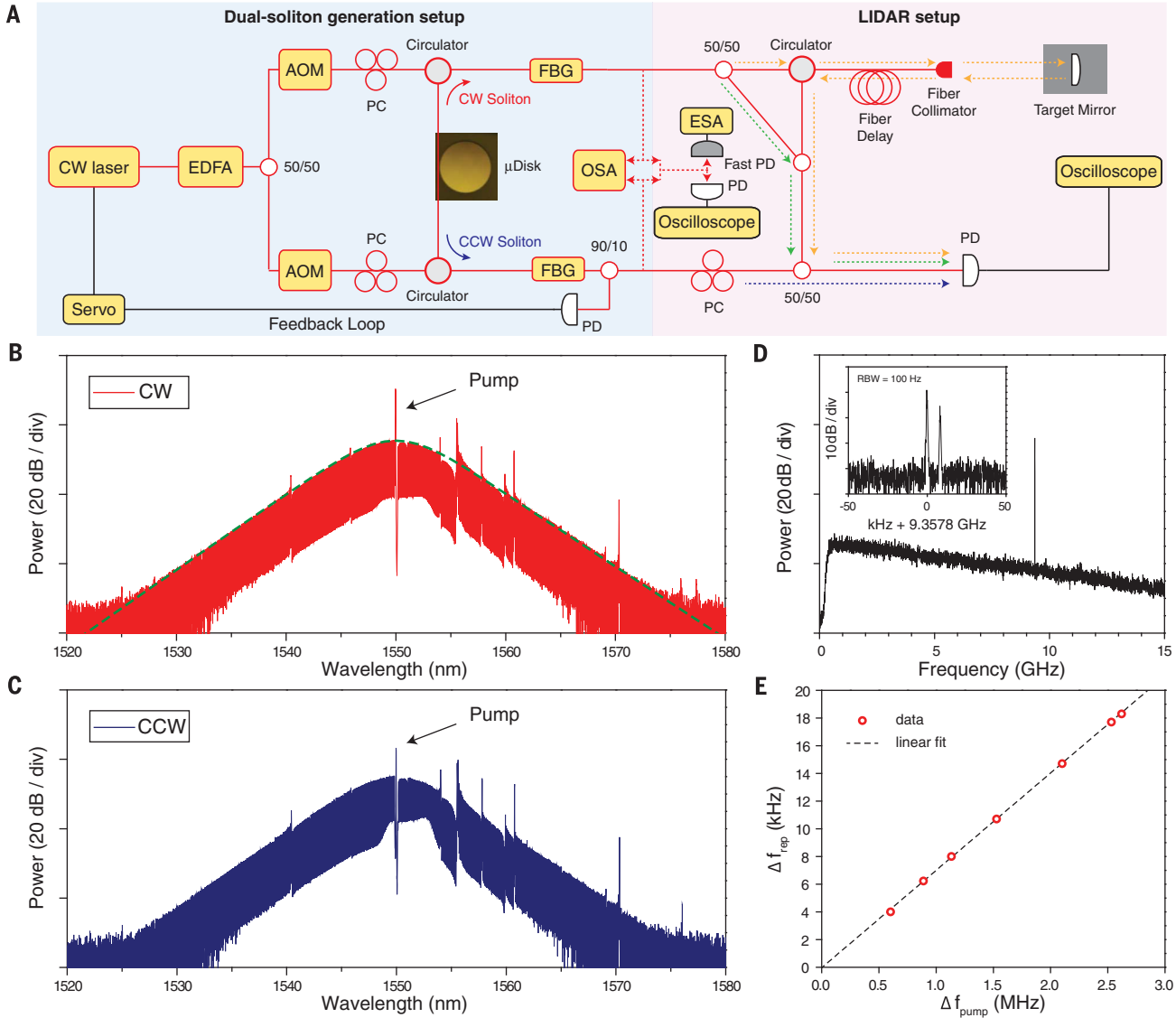

Fig. 1. Experimental setup for dual-soliton generation and ranging measurement. (**A**) The dual-soliton generation setup (left) and LIDAR setup (right). A fiber laser at 1550 nm is amplified by an erbium-doped fiber amplifier (EDFA) and split using a 50/50 coupler to pump the resonator in two directions. In each path, an acousto-optic modulator (AOM) tunes the pump frequency and modulates the pump power for soliton triggering. The pump light is polarization-controlled (PC) and evanescently coupled into the microresonator by means of a fiber taper. Solitons are stabilized and the pump laser frequency locked to the resonator by a servo feedback loop using the photodetected (PD) CCW soliton power (*27*). A fiber Bragg grating (FBG) filter is used to attenuate the transmitted pump power. An optical spectrum analyzer (OSA) and electrical spectrum analyzer (ESA) are used to analyze the dual-soliton source. For distance detection, the CW soliton stream is split into two paths: the reference path (green dashed arrow) and the target path (orange dashed arrow). In the data, the distance difference between the target and reference paths is divided by 2. The CW soliton streams of both paths are combined with the CCW soliton stream (blue dashed arrow) and photodetected to generate the interferogram. (**B** and **C**) Typical optical spectra of the CW solitons (B) and CCW solitons (C) with hyperbolic-secant-square fit [green dashed curve in (B)]. Attenuated pump laser lines are also indicated. (**D**) Electrical spectrum of the photodetected solitons showing the approximate repetition frequency f_{rep} ~ 9.36 GHz. Inset: Zoom-in of the spectrum showing the resolved CW/CCW repetition rates. (**E**) Measured repetition frequency difference Δf_{rep} versus pump frequency difference Δf_{pump}.

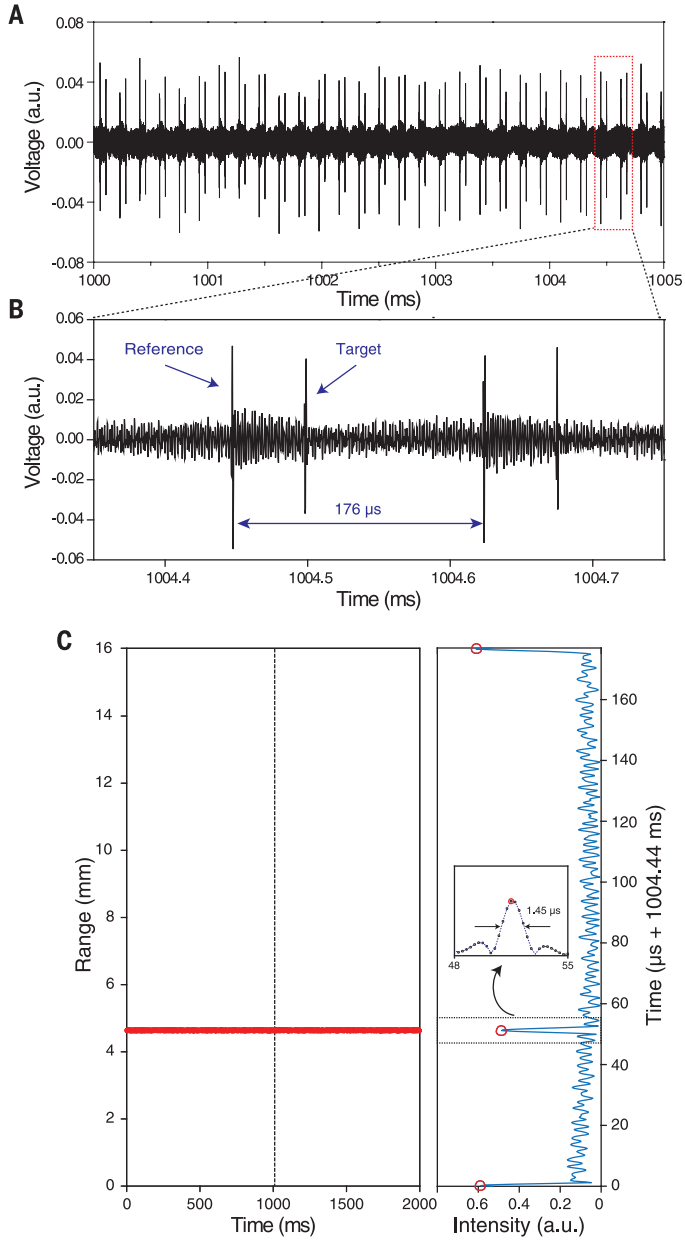

Fig. 2. Distance measurement. (**A**) Typical interferogram containing range information. (**B**) Zoom-in of the interferogram over two time periods. The reference peaks and target peaks are shown; the time period is approximately 176 μs. (**C**) Left: The measured distance between the reference peak and target peak is plotted versus time. The range ambiguity in this measurement is 16 mm. Right: The electrical intensity trace (blue) and peaks (red circles) for a data trace near 1 s (dashed vertical line in left panel). Inset: Zoom-in of the target intensity peak showing the electrical pulse width of 1.45 μs.

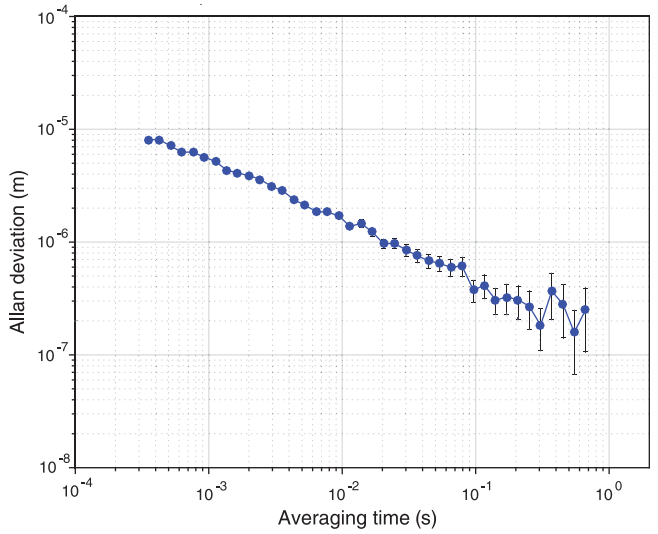

Fig. 3. Precision of distance measurement versus averaging time. Allan deviation is calculated from the 2-s time series (Fig. 2C) of measured distance (i.e., reference peak to signal peak); 200-nm precision is achieved near an averaging time of 500 ms. Error range is calculated from the Allan deviation divided by the square root of sample size.

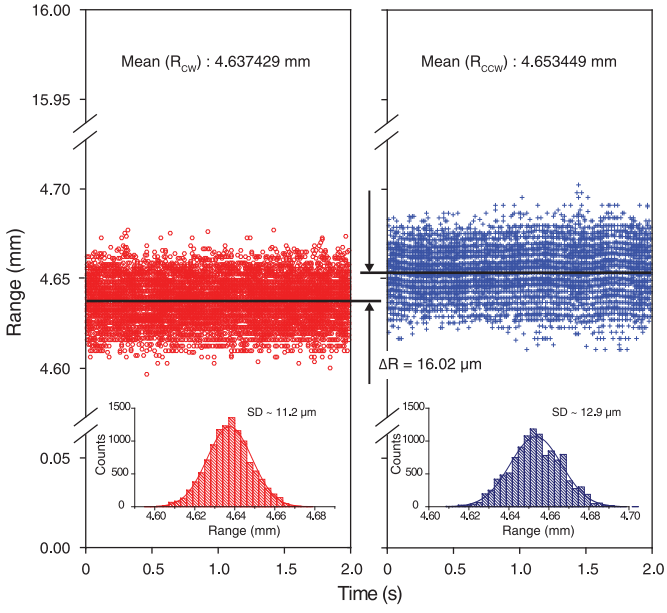

Fig. 4. Resolving range ambiguity. R_{CW} (red) and R_{CCW} (blue) are range data versus time, using the CW and CCW solitons to probe the target. The distance difference [ΔR = mean(R_{CW}) − mean(R_{CCW})] between the two measurements is 16.02 μm and is used to determine the absolute range (see text). Data in red are from Fig. 2C. Insets: Histograms of the two range measurements for one measurement frame, along with the Gaussian fitting curves with standard deviation (SD) values. Standard deviation improves with averaging time as per Fig. 3.

allowing greater averaging of distance data within a given time interval. Achieving the larger range measurements in free space would require optical amplification; in the case of outdoor ranging (*32*), the precision will also be limited by environmental perturbation (*33*).

The update time of ~176 μs and the range ambiguity of ~26 km are determined by Δf_{rep} = 5.685 kHz, which can be tuned by changing Δf_{pump}. The tunable range and absolute value of Δf_{rep} can be further increased by using a smaller-diameter resonator and generating CW/CCW solitons from two different mode families (*30*). The tunability of Δf_{rep} is useful in that the LIDAR system can be adjusted to provide an optimal update time and range ambiguity according to the application. For example, in applications requiring faster update rates, increasing Δf_{rep} improves the update time while reducing the range ambiguity. Our demonstration of a soliton dual-comb LIDAR system using a single, chip-based microresonator pumped by a single laser is a step toward miniaturization of dual-comb ranging systems. Other chip-based components are required

in a full system. Along these lines, there is remarkable progress on realization of microcomb systems (*20*). Moreover, a waveguide-integrated structure comparable in performance to that used in this work has recently been demonstrated (*34*). Finally, we note other soliton microcomb range measurement work (*35*) that was reported while we were preparing this manuscript.

REFERENCES AND NOTES

1. Y. Salvadé, N. Schuhler, S. Lévêque, S. Le Floch, *Appl. Opt.* **47**, 2715–2720 (2008).
2. E. Baumann *et al.*, *Opt. Lett.* **38**, 2026–2028 (2013).
3. I. Coddington, W. Swann, L. Nenadovic, N. Newbury, *Nat. Photonics* **3**, 351–356 (2009).
4. S.-J. Lee, B. Widiyatmoko, M. Kourogi, M. Ohtsu, *Jpn. J. Appl. Phys.* **40**, L878–L880 (2001).
5. P. Del'Haye *et al.*, *Nature* **450**, 1214–1217 (2007).
6. T. J. Kippenberg, R. Holzwarth, S. A. Diddams, *Science* **332**, 555–559 (2011).
7. I. S. Grudinin, N. Yu, L. Maleki, *Opt. Lett.* **34**, 878–880 (2009).
8. S. B. Papp, S. A. Diddams, *Phys. Rev. A* **84**, 053833 (2011).
9. Y. Okawachi *et al.*, *Opt. Lett.* **36**, 3398–3400 (2011).
10. J. Li, H. Lee, T. Chen, K. J. Vahala, *Phys. Rev. Lett.* **109**, 233901 (2012).
11. B. Hausmann, I. Bulu, V. Venkataraman, P. Deotare, M. Lončar, *Nat. Photonics* **8**, 369–374 (2014).
12. L. Razzari *et al.*, *Nat. Photonics* **4**, 41–45 (2010).
13. F. Ferdous *et al.*, *Nat. Photonics* **5**, 770–776 (2011).
14. H. Jung, C. Xiong, K. Y. Fong, X. Zhang, H. X. Tang, *Opt. Lett.* **38**, 2810–2813 (2013).
15. T. Herr *et al.*, *Nat. Photonics* **8**, 145–152 (2014).
16. X. Yi, Q.-F. Yang, K. Y. Yang, M.-G. Suh, K. Vahala, *Optica* **2**, 1078 (2015).
17. V. Brasch *et al.*, *Science* **351**, 357–360 (2016).
18. P.-H. Wang *et al.*, *Opt. Express* **24**, 10890–10897 (2016).
19. C. Joshi *et al.*, *Opt. Lett.* **41**, 2565–2568 (2016).
20. D. T. Spencer *et al.*, arXiv:1708.05228 (2017).
21. P. Marin-Palomo *et al.*, *Nature* **546**, 274–279 (2017).
22. M.-G. Suh, Q.-F. Yang, K. Y. Yang, X. Yi, K. J. Vahala, *Science* **354**, 600–603 (2016).
23. A. Dutt *et al.*, arXiv:1611.07673 (2016).
24. N. G. Pavlov *et al.*, *Opt. Lett.* **42**, 514–517 (2017).
25. Q.-F. Yang, X. Yi, K. Y. Yang, K. Vahala, *Nat. Photonics* **11**, 560–564 (2017).
26. H. Lee *et al.*, *Nat. Photonics* **6**, 369–373 (2012).
27. X. Yi, Q.-F. Yang, K. Y. Yang, K. Vahala, *Opt. Lett.* **41**, 2037–2040 (2016).
28. Q.-T. Cao *et al.*, *Phys. Rev. Lett.* **118**, 033901 (2017).
29. L. Del Bino, J. M. Silver, S. L. Stebbings, P. Del'Haye, *Sci. Rep.* **7**, 43142 (2017).
30. See supplementary materials.
31. T.-A. Liu, N. R. Newbury, I. Coddington, *Opt. Express* **19**, 18501–18509 (2011).
32. J. Lee, Y.-J. Kim, K. Lee, S. Lee, S.-W. Kim, *Nat. Photonics* **4**, 716–720 (2010).
33. N. Bobroff, *Meas. Sci. Technol.* **4**, 907–926 (1993).
34. K. Y. Yang *et al.*, arXiv:1702.05076 (2017).
35. P. Trocha *et al.*, arXiv:1707.05969 (2017).

ACKNOWLEDGMENTS

We thank N. Newbury, X. Yi, and Q. Yang for helpful discussions and feedback on this manuscript. Supported by the Defense Advanced Research Projects Agency under the SCOUT (contract no. W911NF-16-1-0548) program, the Air Force Office of Scientific Research, and the Kavli Nanoscience Institute.

SUPPLEMENTARY MATERIALS

www.sciencemag.org/content/359/6378/884/suppl/DC1
Supplementary Text
Fig. S1
Reference (*36*)

26 June 2017; accepted 11 January 2018
10.1126/science.aao1968

Soliton microcomb range measurement

Myoung-Gyun Suh and Kerry J. Vahala

Science **359** (6378), 884-887.
DOI: 10.1126/science.aao1968

Miniaturized optical ranging and tracking

Light detection and ranging systems are used in many engineering and environmental sensing applications. Their relatively large size and cost, however, tend to be prohibitive for general use in autonomous vehicles and drones. Suh and Vahala and Trocha *et al.* show that optical frequency combs generated by microresonator devices can be used for precision ranging and the tracking of fast-moving objects. The compact size of the microresonators could broaden the scope for widespread applications, providing a platform for miniaturized laser ranging systems suitable for photonic integration.

Science, this issue p. 884, p. 887